Supplementary Information for

Contrasting vertical ozone evolution between coastal and inland sites within a subtropical coastal city: roles of photochemistry and transport during typhoon-influenced weather

Shaojie Jiang[#], Xinlei Ge[#], Dongyang Nie[#], Xiangpeng Huang, Wei Zheng, Honglong Yang, Yaying Wang, Yan Yang, Weifeng Su, Linqiang Ma, Tianzeng Chen, Yanli Zhang, Shutong Jiang, Qiyuan Wang, Junfeng Wang, Chanfang Liu, Lei Zhu, Zhenzhong Zeng, Tzung-May Fu, Xin Yang, Jianhuai Ye*

#These authors contributed equally to the study.

*Correspondence to
Jianhuai Ye (yejh@sustech.edu.cn), ORCID 0000-0002-9063-3260

The Supplementary Information includes 3 supporting texts, 5 tables, and 7 figures.

Text S1 VOC chemical analysis and quality assurance and quality control

Volatile organic compounds (VOCs) collected at Site 1 were analyzed offline using thermal desorption–gas chromatography–mass spectrometry (TD-GC-MS; GERSTEL TD3.5+ coupled to an Agilent 7890B gas chromatograph and 7000D mass spectrometer). During thermal desorption, samples were initially held at 30 °C for 2 min and subsequently heated to 280 °C at 300 °C min^{-1}, followed by a 5 min hold to ensure complete desorption. Desorbed VOCs were cryofocused in a cooling injection system (CIS) maintained at −30 °C and equipped with an activated carbon liner, and were subsequently transferred to the GC following rapid heating of the CIS to 320 °C (10 °C s^{-1}, 10 min hold). Compound separation was performed using an HP-5MS capillary column (60 m × 0.25 mm × 0.25 μm) with a constant carrier-gas flow of 1 mL min^{-1}. The GC oven was initially held at 30 °C for 5 min and then heated to 280 °C at 9 °C min^{-1}, followed by a post-run bakeout at 300 °C for 2 min to ensure complete elution of residual compounds. VOCs were detected by electron-impact mass spectrometry with an ion source temperature of 230 °C and a scanning mass range of m/z 35–250.

Target VOCs at Site 1 were identified using chromatographic retention information and characteristic mass spectra and were quantified using compound-specific calibration curves. For the calibrated compounds, calibration-curve correlation coefficients ranged from 0.9365 to 0.9999, and method detection limits were generally 5 to 22 ppt. A total of 77 VOC species were included in the subsequent analyses at Site 1.

VOCs at Site 2 were measured using an online gas chromatography–mass spectrometry/flame ionization detection system (GC-MS/FID; TH-300B, Wuhan Tianhong Ltd., China). The system used a dual-channel sampling and cryogenic preconcentration configuration. Ambient air was continuously introduced into the sampling line, and VOCs were enriched after removal of water vapor and CO_2. The target compounds were concentrated in an ultra-low-temperature cold trap maintained at -180 °C and were subsequently released by rapid thermal desorption at 150 °C. The desorbed VOCs were transferred to the GC-MS/FID system using helium as the carrier gas. C_2 to C_5 hydrocarbons were separated on a PLOT (Al_2O_3/KCl) column (15 m, 0.32 mm ID) and detected by FID, whereas heavier hydrocarbons and other VOCs were separated (>C_5, DB-624 column, 30 m, 0.25 mm ID) and quantified using the MS detector. External standards were injected weekly, and multipoint calibration was performed every two weeks to ensure data quality.

Method detection limits were approximately 5 ppt for most measured species, and the overall

sampling and analytical uncertainty was <15 %. The VOC species included in the analyses at the two sites and their representation in the Master Chemical Mechanism (MCM) v3.3.1 are summarized in Table S3. The Site 2 analytical system covered 116 VOC species (Wang et al., 2014), of which 93 were included in the analyses. Independent site analyses used all available species; direct cross-site comparisons used only species measured by both systems. Of the 77 Site 1 species and 93 Site 2 species included in the analyses, 55 and 65, respectively, were represented in MCM, with 44 common MCM-represented species (Table S3).

Text S2 UAV observations during the 2022 field campaign

During the 2022 campaign, vertical profiles were typically obtained using a DJI M300 UAV at 09:00, 11:00, 14:00, 16:00, 19:00, and 21:00 local time. Measurements were conducted over the ocean approximately 100 m from the shoreline. O_x, NO_2, CO, $PM_{2.5}$, and PM_{10} were measured using a Sniffer4D V2 sensor package. As in 2023, the sensors were collocated with ground-based reference instruments when the UAV was not in flight and calibrated using Random Forest regression with sensor signals, temperature, and relative humidity as predictors. The model used 500 trees, a maximum depth of 10, and a minimum of five samples to split an internal node, with other parameters at their default values. VOC measurements were not conducted during the 2022 campaign.

Text S3 Backward-trajectory calculation and air-mass pathway classification

To characterize the recent regional transport history of air masses sampled at Site 1, 12 h backward trajectories were calculated using the Hybrid Single-Particle Lagrangian Integrated Trajectory (HYSPLIT) model driven by 1° Global Data Assimilation System (GDAS1) meteorological fields. Trajectories were initialized at 500 m above ground level (AGL) over Site 1 for both the 2022 and 2023 campaigns. A 12 h duration was selected to emphasize transport immediately preceding each UAV observation rather than long-range source attribution, for which longer trajectories would introduce greater trajectory uncertainty. A common receptor height of 500 m AGL was used for both campaigns to maintain consistent trajectory settings between the two datasets and to characterize regional transport into the upper part of the lower troposphere.

For each trajectory, coordinates were extracted at hourly intervals from 1 to 12 h before arrival.

Each trajectory position was classified as being over land or ocean using the Natural Earth land mask. The land fraction was calculated as follows.

$$f_{land} = \frac{N_{land}}{N_{land} + N_{ocean}}$$

where N_{land} and N_{ocean} represent the numbers of hourly trajectory positions over land and ocean, respectively. Profiles with $f_{land} < 0.5$ were classified as marine-pathway air masses, those with $f_{land} > 0.5$ as land-pathway air masses, and cases with $f_{land} = 0.5$ as transitional and excluded from the binary comparison. The 0.5 threshold therefore represents a simple majority classification of the recent regional transport pathway.

The same 12 h trajectory duration, 500 m receptor height, land-mask procedure, and pathway-classification criteria were applied to all valid profiles in both campaigns. The classified profiles are listed in Table S4. The 2023 campaign provided the primary analysis, while the longer 2022 campaign provided an additional comparison of pathway-dependent pollutant distributions.

Table S1 Summary of instruments used for UAV observations and ground-based measurements.

Instruments	Measurement variables	Temporal resolution	Measurement range	Detection limit or accuracy
POM	O_3	2 s	0 ppb to 10 ppm	3 ppb
Sniffer 4D sensor package	O_x	1 s	0 to 11 ppm	5 ppb
	NO_2	1 s	0 to 11 ppm	5 ppb
	CO	1 s	0 to 11 ppm	4 ppb
	$PM_{2.5}$ and PM_{10}	1 s	0 to 1000 μg m^{-3}	1 μg m^{-3}
	wind speed	1 s	0 to 50 m s^{-1}	± 0.1 m s^{-1} (0 to 10 m s^{-1}) ± 1 m s^{-1} (11 to 30 m s^{-1}) ± 2 m s^{-1} (31 to 50 m s^{-1})
	wind direction	1 s	0 to 360°	1.0°
HOBO logger	temperature	1 s	-40 to 70°C	0.02°C
	relative humidity	1 s	0 to 100%	1%
Thermo Scientific 49i	O_3	60 s	0 to 200 ppm	0.50 ppb
Thermo Scientific 42i	NO, NO_2, NO_x	60 s	0 to 100 ppm	0.40 ppb
Thermo Scientific 48i	CO	60 s	0 to 20000 ppm	0.04 ppm
Thermo Scientific 5030 SHARP	$PM_{2.5}$ and PM_{10}	60 s	0 to 10 mg m^{-3}	<0.5 μg m^{-3} (1 h, 2σ) <0.2 μg m^{-3} (24 h, 2σ)

Table S2 Random Forest calibration performance and residual-based uncertainty metrics for UAV pollutant measurements during the 2023 campaign. R^2 and slope are dimensionless. Intercept, root mean square error (RMSE), mean bias error (MBE), and the 95 % residual interval are reported in the corresponding concentration units, μg m^{-3} for O_3, NO_2, $PM_{2.5}$, and PM_{10}, and mg m^{-3} for CO. Residuals were calculated as the differences between Random Forest-predicted concentrations and measurements from the collocated reference instruments. All metrics and residual intervals were calculated using the held-out test set, which comprised 20 % of the samples.

Pollutant	R^2	Slope	Intercept	RMSE	MBE	95% residual interval
O_3	0.95	0.95	5.39	12.62	0.06	[-27.83, 27.64]
CO	0.75	0.73	0.21	0.05	-0.01	[-0.12, 0.08]
NO_2	0.70	0.69	2.96	4.14	0.08	[-6.77, 6.79]
$PM_{2.5}$	0.92	0.90	1.28	2.31	-0.14	[-5.87, 3.94]
PM_{10}	0.93	0.89	2.36	3.30	-0.28	[-9.03, 6.68]

Table S3 VOC species included in the analyses at Sites 1 and 2 and their representation in MCM.

VOC species	Site 1	Site 2	MCM
1,1,1-Trichloroethane	✓	✓	✓
1,1,2,2-Tetrachloroethane	✓	✓	✓
1,1,2-trichloro-1,2,2-trifluoroethane	✓	✓	-
1,1,2-Trichloroethane	✓	✓	✓
1,1-Dichloroethane	✓	✓	✓
1,1-Dichloroethene	✓	✓	✓
1,2,3-Trimethylbenzene	✓	✓	✓
1,2,4-Trichlorobenzene	✓	-	-
1,2,4-Trimethylbenzene	✓	✓	✓
1,2-Dibromoethane	✓	✓	✓
1,2-Dichlorobenzene	✓	✓	-
1,2-Dichloroethane	-	✓	✓
1,2-Dichloropropane	-	✓	✓
1,2-Dichlorotetrafluoroethane	-	✓	-
1,3,5-Trimethylbenzene	✓	✓	✓
1,3-Butadiene	-	✓	✓
1,3-Dichlorobenzene	✓	✓	-
1,4-Dichlorobenzene	✓	✓	-
1-Butene	-	✓	✓
1-Hexene	✓	✓	✓
2,2,4-Trimethylpentane	✓	✓	-
2,2-Dimethylbutane	✓	✓	✓
2,3,4-Trimethylpentane	✓	✓	-
2,3-Dimethylbutane	-	✓	✓
2,3-Dimethylpentane	✓	✓	-
2,4-Dimethylpentane	✓	✓	-
2-Hexanone	✓	-	✓
2-Methylheptane	-	✓	-
2-Methylhexane	✓	✓	✓
2-Methylpentane	✓	-	✓
3-Methylheptane	-	✓	-
3-Methylhexane	✓	✓	✓
3-Methylpentane	✓	✓	✓
α-pinene	✓	-	✓
Acetaldehyde	-	✓	✓
Acetone	✓	✓	✓
Acetylene	-	✓	✓
Acrolein	-	✓	✓

VOC species	Site 1	Site 2	MCM
Benzene	✓	✓	✓
Bromodichloromethane	✓	✓	-
Bromoform	✓	✓	-
Bromomethane	-	✓	✓
Butyraldehyde	✓	✓	✓
Carbon disulfide	✓	✓	-
Carbon tetrachloride	✓	✓	-
Chlorobenzene	✓	✓	-
Chloroethane	-	✓	✓
Chloroform	✓	✓	✓
Chloromethane	-	-	-
cis-1,2-Dichloroethene	✓	✓	✓
cis-1,3-Dichloropropene	✓	✓	-
cis-2-Butene	-	-	-
cis-2-Pentene	✓	-	✓
Crotonaldehyde	-	✓	-
Cyclohexane	-	✓	✓
Cyclopentane	-	✓	-
Dibromochloromethane	✓	✓	-
Dichlorodifluoromethane	-	✓	-
Ethane	-	✓	✓
Ethyl acetate	✓	✓	✓
Ethylbenzene	✓	✓	✓
Ethylene	-	✓	✓
Hexachloro-1,3-Butadiene	✓	-	-
Isobutane	-	✓	✓
Isopentane	-	✓	✓
Isoprene	✓	✓	✓
IsopropylAlcohol	✓	-	✓
Isopropylbenzene	✓	✓	✓
limonene	✓	-	✓
m-Diethylbenzene	✓	-	-
m-Ethyltoluene	✓	✓	✓
m-Tolualdehyde	-	-	-
m-Xylene	✓	✓	✓
MEK	✓	✓	✓
Methacrolein (MACR)	✓	✓	✓
Methyl methacrylate	✓	✓	-
Methylcyclohexane	✓	✓	-
Methylcyclopentane	-	✓	-

VOC species	Site 1	Site 2	MCM
Methylene chloride	✓	✓	✓
MethylisobutylKetone	✓	-	✓
MTBE	✓	✓	✓
MVK	✓	-	✓
n-Butane	-	✓	✓
n-Decane	✓	✓	✓
n-Dodecane	✓	-	✓
n-Heptane	-	✓	✓
n-Hexane	✓	✓	✓
n-Nonane	✓	✓	✓
n-Octane	✓	✓	✓
n-Pentane	✓	✓	✓
n-Propylbenzene	✓	✓	✓
n-Undecane	✓	-	✓
Naphthalene	✓	-	-
o-Ethyltoluene	✓	✓	✓
o-Xylene	✓	✓	✓
p-Diethylbenzene	✓	-	-
p-Ethyltoluene	✓	✓	✓
p-Xylene	✓	✓	✓
Propane	-	✓	✓
Propylene	-	✓	✓
Styrene	✓	✓	✓
Tetrachloroethylene	✓	✓	✓
Tetrahydrofuran	-	✓	-
Toluene	✓	✓	✓
trans-1,2-Dichloroethene	✓	✓	✓
trans-1,3-Dichloropropene	-	✓	-
trans-2-Butene	-	✓	✓
trans-2-Pentene	✓	-	✓
Trichloroethylene	✓	✓	✓
Trichlorofluoromethane	-	✓	-
Vinyl acetate	-	✓	-
Vinyl chloride	-	✓	✓

Table S4 Summary of UAV profiles and air-mass classifications during the 2022 and 2023 campaigns.

Date	Time	Type
2022-08.21	14:00	Marine-pathway air mass
08.21	16:00	Marine-pathway air mass
08.21	19:00	Marine-pathway air mass
08.21	21:00	Marine-pathway air mass
08.22	09:00	Marine-pathway air mass
08.22	11:00	Marine-pathway air mass
08.22	14:00	Marine-pathway air mass
08.22	16:00	Marine-pathway air mass
08.22	19:00	Land-pathway air mass
08.22	21:00	Marine-pathway air mass
08.23	09:00	Land-pathway air mass
08.23	11:00	Land-pathway air mass
08.27	14:00	Land-pathway air mass
08.27	16:00	Land-pathway air mass
08.27	19:00	Marine-pathway air mass
08.27	21:00	Land-pathway air mass
08.28	09:00	Land-pathway air mass
08.28	11:00	Land-pathway air mass
08.28	14:00	Marine-pathway air mass
08.28	16:00	Marine-pathway air mass
08.28	19:00	Marine-pathway air mass
08.28	21:00	Marine-pathway air mass
08.29	09:00	Marine-pathway air mass
08.29	11:00	Marine-pathway air mass
08.29	14:00	Marine-pathway air mass
08.29	16:00	Marine-pathway air mass
08.29	19:00	Marine-pathway air mass
08.29	21:00	Marine-pathway air mass
08.30	09:00	Land-pathway air mass
08.30	11:00	Land-pathway air mass
08.30	14:00	Marine-pathway air mass
08.30	16:00	Marine-pathway air mass
08.30	19:00	Marine-pathway air mass
08.30	21:00	Marine-pathway air mass
08.31	09:00	Land-pathway air mass
08.31	11:00	Land-pathway air mass

Date	Time	Type
08.31	14:00	Land-pathway air mass
08.31	16:00	Marine-pathway air mass
08.31	19:00	Marine-pathway air mass
08.31	21:00	Marine-pathway air mass
09.01	09:00	Land-pathway air mass
09.01	11:00	Land-pathway air mass
09.01	14:00	Land-pathway air mass
09.01	16:00	Land-pathway air mass
09.01	19:00	Land-pathway air mass
09.01	21:00	Land-pathway air mass
09.02	09:00	Land-pathway air mass
09.02	11:00	Land-pathway air mass
09.02	14:00	Land-pathway air mass
09.02	16:00	Land-pathway air mass
09.02	19:00	Land-pathway air mass
09.02	21:00	Land-pathway air mass
09.03	09:00	Land-pathway air mass
09.03	11:00	Land-pathway air mass
09.03	14:00	Land-pathway air mass
09.03	16:00	Land-pathway air mass
09.03	19:00	Land-pathway air mass
09.03	21:00	Land-pathway air mass
09.04	09:00	Land-pathway air mass
09.04	11:00	Land-pathway air mass
09.04	14:00	Land-pathway air mass
09.04	16:00	Land-pathway air mass
09.04	19:00	Land-pathway air mass
09.04	21:00	Land-pathway air mass
09.05	09:00	Land-pathway air mass
09.05	11:00	Land-pathway air mass
09.05	14:00	Land-pathway air mass
09.05	16:00	Land-pathway air mass
09.05	19:00	Land-pathway air mass
09.05	21:00	Land-pathway air mass
09.06	09:00	Land-pathway air mass
09.06	11:00	Land-pathway air mass
09.06	14:00	Marine-pathway air mass
09.06	16:00	Marine-pathway air mass

Date	Time	Type
09.06	19:00	Marine-pathway air mass
09.06	21:00	Marine-pathway air mass
09.07	09:00	Marine-pathway air mass
09.07	11:00	Marine-pathway air mass
09.07	14:00	Marine-pathway air mass
09.07	16:00	Marine-pathway air mass
09.07	19:00	Marine-pathway air mass
09.07	21:00	Marine-pathway air mass
09.08	09:00	Land-pathway air mass
09.08	11:00	Marine-pathway air mass
09.08	14:00	Marine-pathway air mass
09.08	16:00	Marine-pathway air mass
09.08	19:00	Marine-pathway air mass
09.08	21:00	Marine-pathway air mass
09.09	09:00	Land-pathway air mass
09.09	11:00	Land-pathway air mass
09.09	14:00	Marine-pathway air mass
09.09	16:00	Marine-pathway air mass
09.09	19:00	Marine-pathway air mass
09.09	21:00	Marine-pathway air mass
09.13	09:00	Land-pathway air mass
09.13	11:00	Land-pathway air mass
09.13	14:00	Land-pathway air mass
09.13	16:00	Land-pathway air mass
09.13	19:00	Land-pathway air mass
09.13	21:00	Land-pathway air mass
09.14	09:00	Land-pathway air mass
09.14	11:00	Land-pathway air mass
09.14	14:00	Land-pathway air mass
09.14	16:00	Land-pathway air mass
09.14	19:00	Land-pathway air mass
09.14	21:00	Land-pathway air mass
Date	**Time**	**Type**
2023-05.30	8:00	Land-pathway air mass
05.30	11:00	Land-pathway air mass
05.30	14:00	Land-pathway air mass
05.30	15:30	Land-pathway air mass
05.30	17:00	Land-pathway air mass

Date	Time	Type
05.30	20:00	Land-pathway air mass
05.30	21:30	Land-pathway air mass
05.30	23:00	Land-pathway air mass
05.31	08:00	Land-pathway air mass
05.31	09:30	Marine-pathway air mass
05.31	11:00	Marine-pathway air mass
05.31	14:00	Land-pathway air mass
05.31	15:30	Land-pathway air mass
05.31	17:00	Land-pathway air mass
05.31	20:00	Land-pathway air mass
05.31	21:30	Marine-pathway air mass
05.31	23:00	Marine-pathway air mass
06.01	08:00	Marine-pathway air mass
06.01	09:30	Land-pathway air mass
06.01	11:00	Marine-pathway air mass
06.01	14:00	Marine-pathway air mass
06.01	15:30	Marine-pathway air mass
06.01	17:00	Marine-pathway air mass
06.01	20:00	Land-pathway air mass
06.01	21:30	Marine-pathway air mass
06.01	23:00	Marine-pathway air mass
06.02	08:00	Marine-pathway air mass
06.02	09:30	Marine-pathway air mass
06.02	11:00	Marine-pathway air mass
06.02	14:00	Land-pathway air mass
06.02	15:30	Marine-pathway air mass
06.02	17:00	Marine-pathway air mass
06.02	20:00	Marine-pathway air mass
06.02	21:30	Marine-pathway air mass
06.02	23:00	Marine-pathway air mass
06.03	08:00	Marine-pathway air mass
06.03	09:30	Marine-pathway air mass
06.03	11:00	Marine-pathway air mass
06.03	14:00	Marine-pathway air mass
06.03	15:30	Marine-pathway air mass
06.03	17:00	Marine-pathway air mass
06.03	20:00	Marine-pathway air mass
06.03	21:30	Marine-pathway air mass

Date	Time	Type
06.03	23:00	Marine-pathway air mass
06.04	08:00	Marine-pathway air mass
06.04	09:30	Marine-pathway air mass
06.04	11:00	Marine-pathway air mass
06.04	14:00	Marine-pathway air mass
06.04	15:30	Marine-pathway air mass
06.04	17:00	Marine-pathway air mass
06.04	20:00	Marine-pathway air mass
06.04	21:30	Marine-pathway air mass
06.04	23:00	Marine-pathway air mass
06.05	08:00	Marine-pathway air mass
06.05	09:30	Marine-pathway air mass
06.05	11:00	Marine-pathway air mass
06.05	14:00	Marine-pathway air mass
06.05	15:30	Marine-pathway air mass
06.05	17:00	Marine-pathway air mass
06.05	20:00	Marine-pathway air mass
06.05	21:30	Marine-pathway air mass
06.05	23:00	Marine-pathway air mass

Table S5 Same-profile and one-profile-lag relationships between vertical wind-direction contrast and O_3 gradient at Site 1 during the three Stage I days. Here, t denotes a given UAV profiling time, and t+1 denotes the immediately subsequent UAV profile on the same day. For the same-profile analysis, $\Delta\theta(t)$ was paired with $\Delta O_3(t)$; for the one-profile-lag analysis, $\Delta\theta(t)$ was paired with $\Delta O_3(t+1)$. Because the time intervals between successive UAV profiles were not uniform, t+1 represents the next observational profile rather than a fixed physical time lag. $\Delta\theta$ denotes the minimum circular angular difference between layer-mean wind directions in the upper (300–450 m AGL) and lower (0–150 m AGL) layers, and ΔO_3 denotes the corresponding upper-minus-lower layer-mean O_3 difference. Pearson r and the number of paired profiles (n) are reported as descriptive statistics. Correlations were calculated from the original paired profiles.

Date	Relationship	n	Pearson *r*
May 30	$\Delta\theta(t)$ vs $\Delta O_3(t)$	8	0.32
	$\Delta\theta(t)$ vs $\Delta O_3(t+1)$	7	0.66
May 31	$\Delta\theta(t)$ vs $\Delta O_3(t)$	9	0.42
	$\Delta\theta(t)$ vs $\Delta O_3(t+1)$	8	0.51
June 1	$\Delta\theta(t)$ vs $\Delta O_3(t)$	9	0.51
	$\Delta\theta(t)$ vs $\Delta O_3(t+1)$	8	0.82

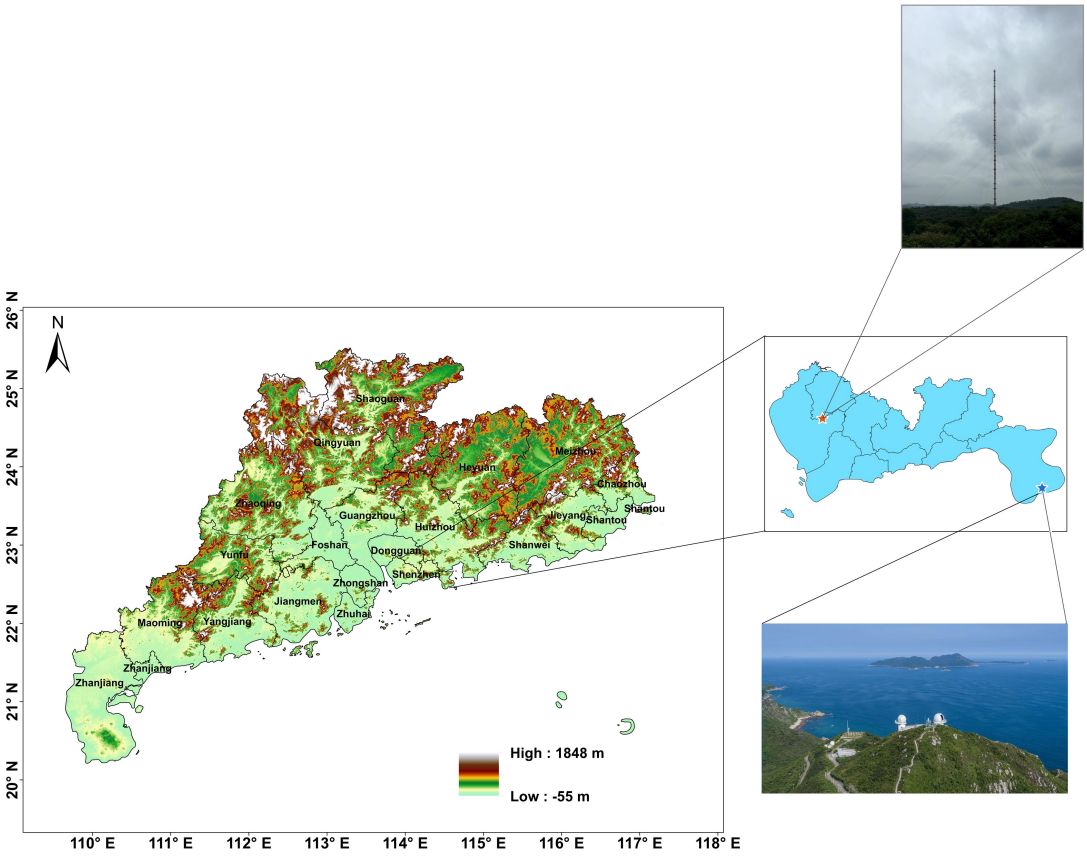


Figure S1 Locations of Site 1 (Shenzhen National Climate Observatory; lower panel) and Site 2 (Shiyan Meteorological Gradient Observation Tower; upper panel).



Figure S2 UAV platforms used for vertical profiling (left) and VOC sampling (right).

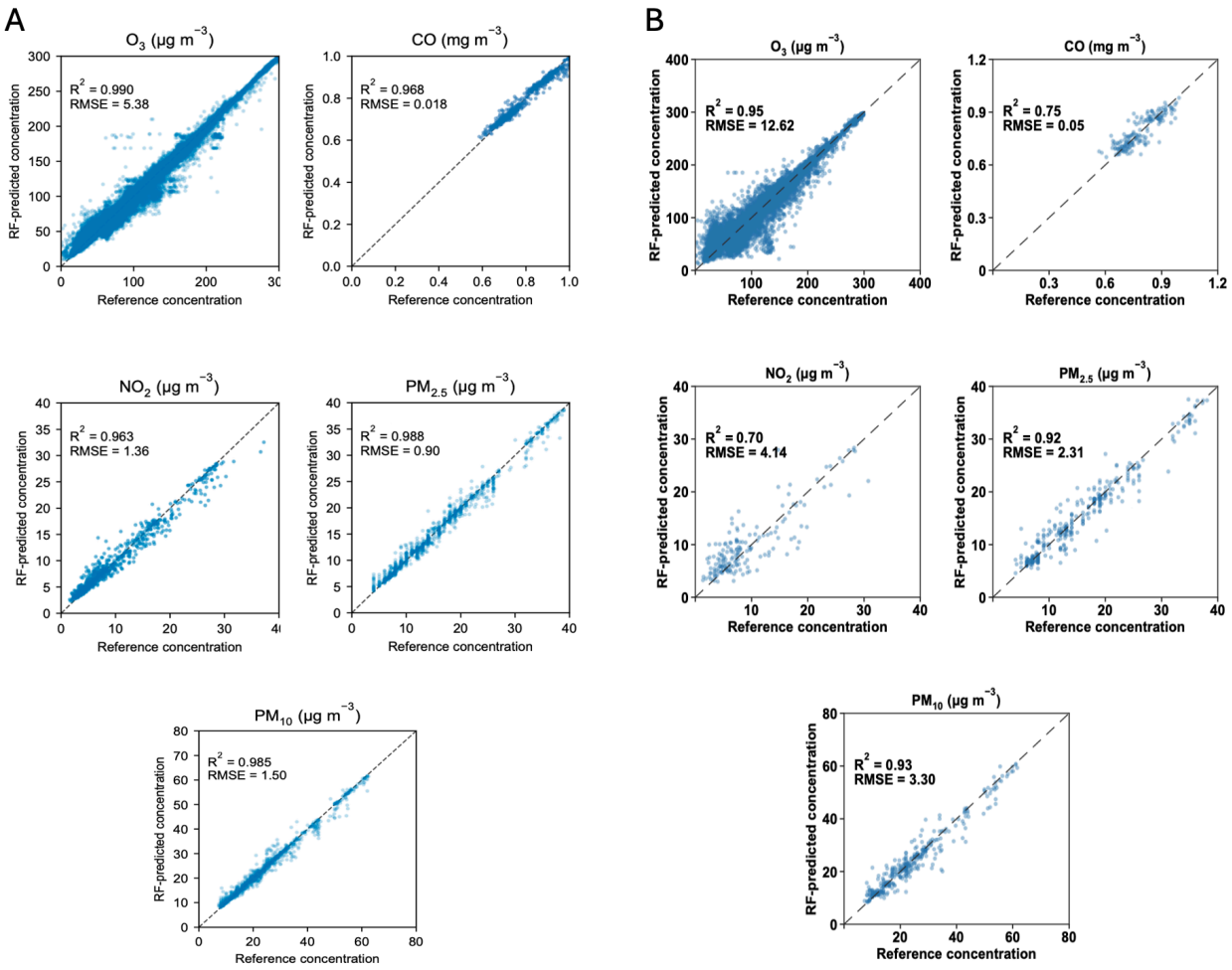


Figure S3 Comparison of Random Forest-predicted and reference-instrument pollutant concentrations for the training set (left) and test set (right). The test set comprised 20% of the samples. Relative humidity and temperature were included as predictor variables alongside the pollutant sensor signals.

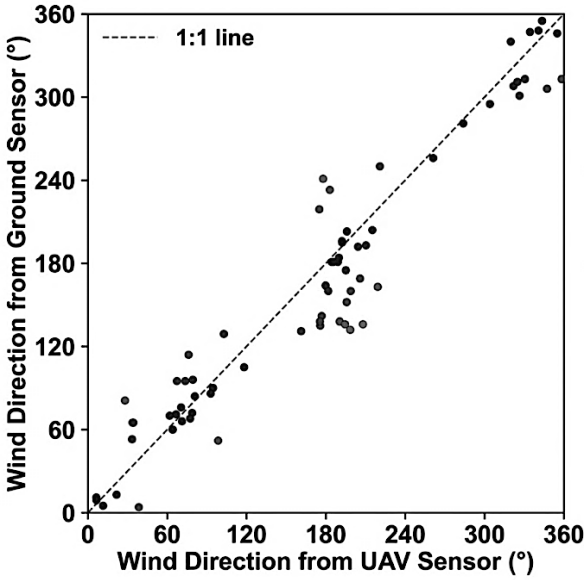


Figure S4 Comparison of wind directions measured by the UAV and the ground-based reference instrument at Site 1. Ground-based wind direction was averaged over the corresponding 5-min period. Only periods when the UAV was operated at the same altitude as the reference sensor during the flights were included in the comparison.

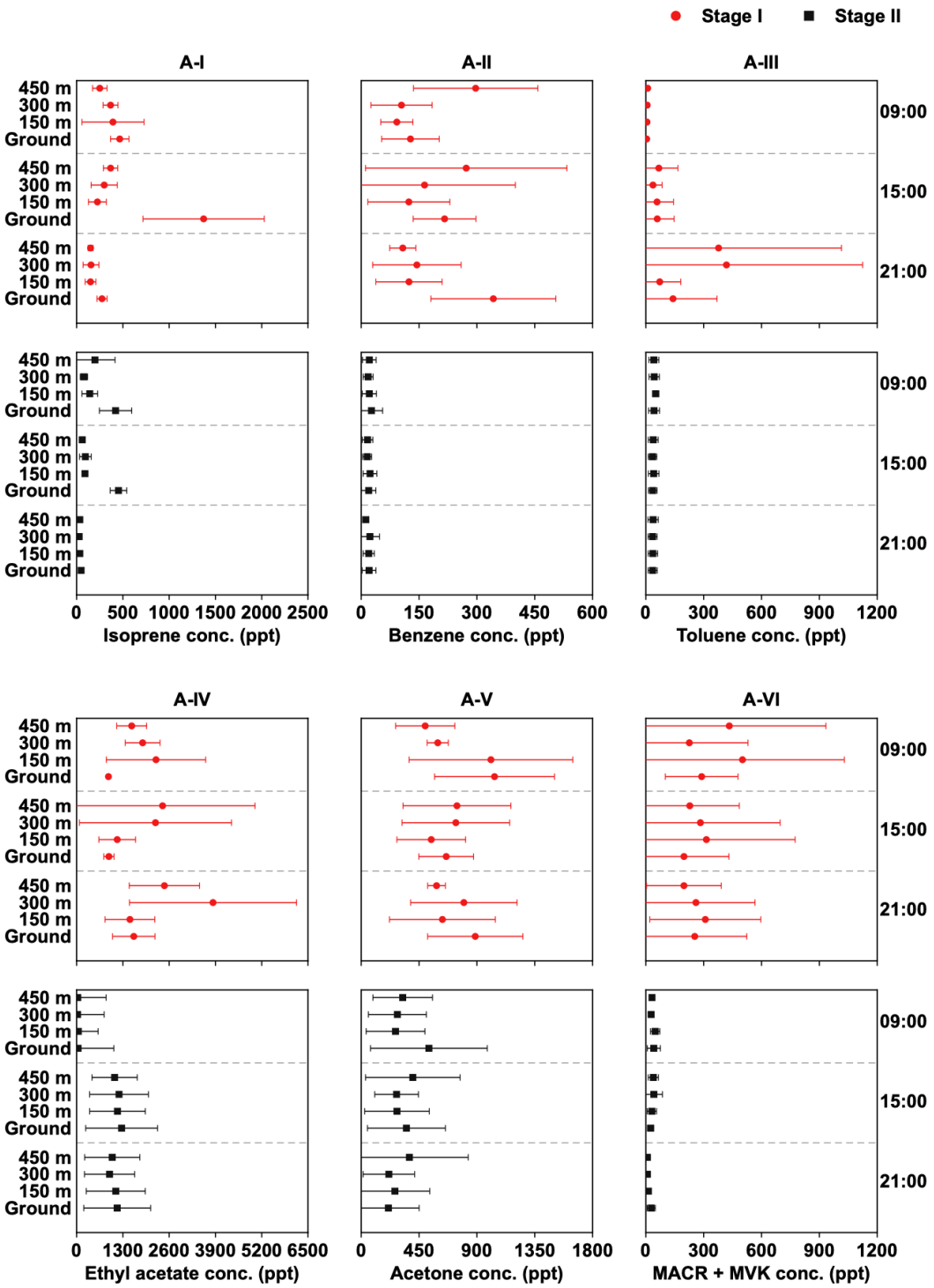
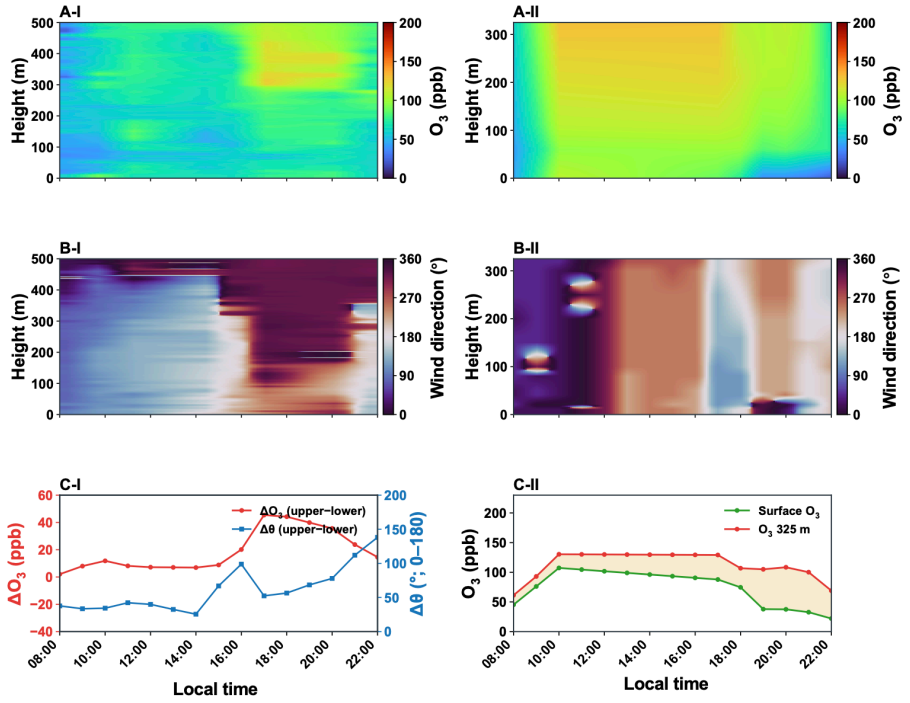


Figure S5 Vertical distributions of selected VOC species observed at Site 1 during Stage I (red points) and Stage II (black points). The error bars indicate ± 1σ standard deviation.

31 May 2023



1 June 2023

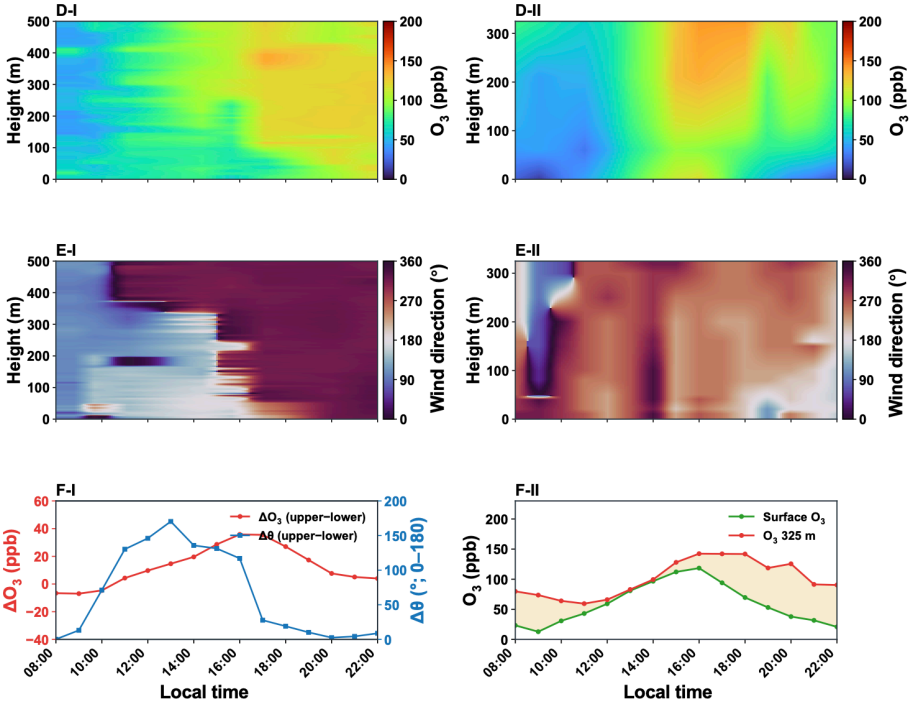


Figure S6 Vertical O_3 evolution and wind-direction structures at Sites 1 and 2 on 31 May and 1 June 2023 during Stage I. Panels A-I to C-II show observations on 31 May, and Panels D-I to F-II show observations on 1 June. Panels A-I, A-II, D-I, and D-II show the time-

height evolution of O_3 at Sites 1 and 2. Panels B-I, B-II, E-I, and E-II show the corresponding time-height evolution of wind direction. Panels C-I and F-I show the temporal evolution of the vertical O_3 difference ΔO_3 and wind-direction difference $\Delta\theta$ at Site 1. ΔO_3 was calculated as the difference between layer-mean O_3 concentrations in the upper 300 to 450 m AGL and lower 0 to 150 m AGL layers, and $\Delta\theta$ represents the minimum circular angular difference from 0 to 180° between the corresponding layer-mean wind directions. Panels C-II and F-II show O_3 concentrations near the surface and at 325 m AGL at Site 2. Interpolation between adjacent profiles and sampling times was used for visualization. Quantitative gradient and correlation analyses were based on the original observations. O_3 mass concentrations in the time-height fields were converted to ppb at standard temperature and pressure.

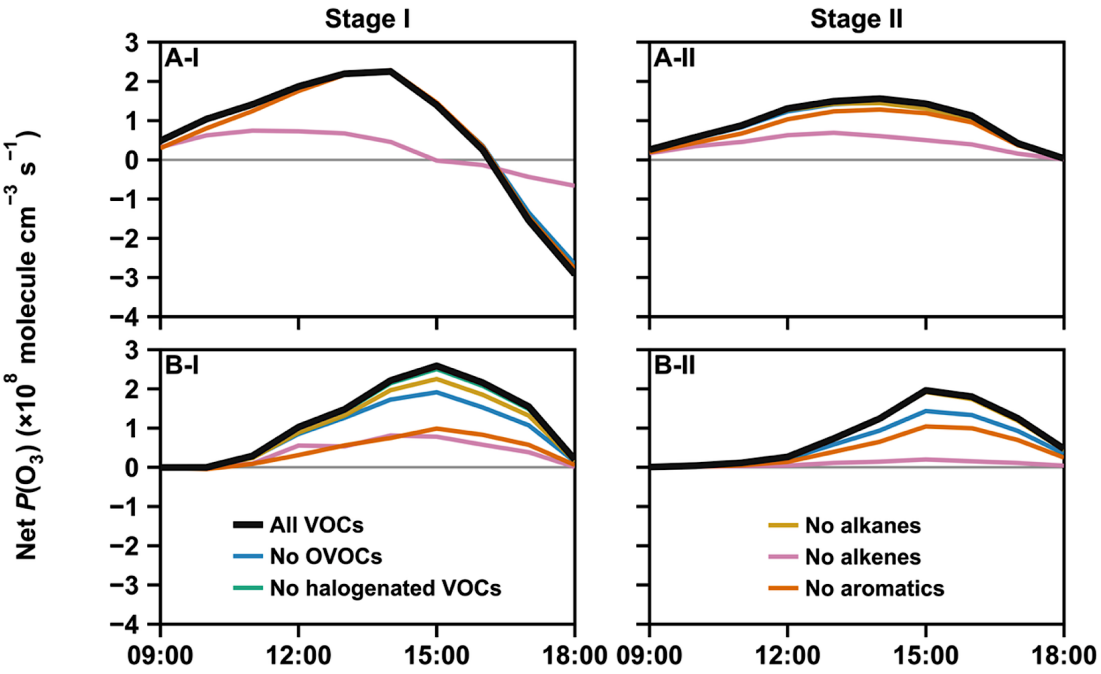


Figure S7 Sensitivity of surface net O_3 production to changes in VOC composition at Sites 1 and 2 during Stage I and Stage II. Panels A-I and A-II show the sensitivity simulations at Site 1 on 30 May 2023 and 4 June 2023, respectively, representing Stage I and Stage II. Panels B-I and B-II show the corresponding simulations at Site 2. The black line represents the simulation constrained by the 44 common MCM-represented VOC species, while the colored lines represent simulations excluding individual VOC classes, including OVOCs, halogenated VOCs, alkanes, alkenes, and aromatics. Differences from the all-VOC simulation indicate the sensitivity of local net O_3 production to the corresponding VOC class.